A 3D SPHEROID MODEL AS A PLATFORM TO STUDY NON-VIRAL GENE DELIVERY SYSTEM

by

Yuzhe Chen

BS, Zhejiang University, College of Pharmaceutical Science, 2009

Submitted to the Graduate Faculty of

School of Pharmacy in partial fulfillment

of the requirements for the degree of

Master of Science

University of Pittsburgh

2015

UNIVERSITY OF PITTSBURGH

School of Pharmacy

This thesis was presented

by

Yuzhe Chen

It was defended on

July 23, 2015

and approved by

Dr. Shilpa Sant, Assistant Professor, School of Pharmacy

Dr. Jiang Li, Associated Professor, School of Pharmacy

Dr. Vinayak Sant, Assistant Professor, School of Pharmacy

Thesis Director Advisor: Dr. Shilpa Sant, Assistant Professor, School of Pharmacy

A 3D SPHEROID MODEL AS A PLATFORM TO STUDY NON-VIRAL GENE DELIVERY SYSTEM

Yuzhe Chen, BS

University of Pittsburgh, 2015

Non-viral gene delivery has emerged as a promising strategy in the past two decades for gene therapy. However, it is difficult to translate non-viral gene delivery into clinical trials. This is because of the low transfection efficiency of non-viral vectors and little knowledge about transfection mechanism in 3D tissues. The complex microenvironment of 3D tissues results in the poor relevance of non-viral transfection in conventional 2D monolayer cells and 3D tissues. Here, we develop a 3D multicellular spheroid model to increase the understanding of the gene delivery process by non-viral vectors in 3D tissues. We synthesized Spermine-conjugated-Dextran (SD), non-viral vector, for gene delivery to 3D tissues. Then, we utilized micro-fabrication technique to prepare 3D spheroids with uniform size in a high throughput manner. We compared the transfection of SD/DNA nanocomplexes in 2D cells and 3D spheroids. Our results revealed that the transfection efficiency and cytotoxicity of non-viral vectors were lower in 3D spheroids than those in 2D monolayer cells. We used confocal microscopy to visualize the cellular uptake of SD/DNA complex in monolayer cells and spheroids. The results demonstrated that SD vector was limited to the external layers of cells in 3D spheroids and couldn't penetrate into the core of spheroids. Taken together, our study indicates that the non-viral transfection behavior in 3D spheroid model is different from that in 2D cells, and this model may be more relevant to *in vivo* setting than that of conventional 2D monolayer cell models. This system also provides a useful high throughput *in vitro* screening platform for the novel non-viral gene delivery system testing in the future.

TABLE OF CONTENTS

LIST OF FIGURES

ACKNOWLEDGEMENTS

I would like to express my sincere thanks to University of Pittsburgh, School of Pharmacy, for giving me the opportunity to study pharmaceutical science here. I thank my advisor Dr. Shilpa Sant for guiding me throughout my graduate studies. I would like to thank Dr. Vinayak Sant for his support and guidance.

I sincerely thank Dr. Manjulata Singh and Dr. Kishor Sarkar for their kind help in my research and thesis writing.

I sincerely thank my friends Shilpaa Mukundan, Yingfei Xue, Akhil Patel, Harini Krishnan, Jean Jr. Liu and other lab members from Dr. Sant's lab for their support and encouragement.

I also sincerely thank all the faculty, staff and fellow graduate students from the School of Pharmacy.

Finally, I am immensely grateful to my parents and my fiancée Miss Bing Huang, who have always been a great support and source of encouragement to me.

1.0 INTRODUCTION

The success of gene therapy largely depends on the delivery system, which should have desired transfection efficiency with low cytotoxicity. Despite the high transfection efficiency of viral vectors, the safety concerns such as carcinogenesis, immunogenicity and risks of mutation have limited their use clinically [2, 3]. As a result, non-viral vectors have gained tremendous attention as an alternative delivery system due to their non-immunogenicity, ease of modification, low toxicity and low production cost. Unfortunately, even if non-viral systems show good transfection efficiency in cultured monolayer two dimensional (2D) cell lines *in vitro*, the efficacy of *in vivo* non-viral gene delivery is not sufficient to provide therapeutic benefits. Due to the complex microenvironment *in vivo,* very little is known about the mechanism of gene delivery in *in vivo* tissues with three dimensional (3D) architectures. The obstacle in solving this problem is the poor relevance of non-viral transfection in conventional 2D monolayer cells and 3D tissues. Therefore, it is urgent to develop more relevant *in vitro* models for studying the gene delivery in 3D tissues in *vitro* as well as for screening the newly developed non-viral gene delivery systems prior to the pre-clinical *in vivo* study.

3D multicellular spheroids of stem cells and cancer cells have been generated for tissue regeneration [12] and anti-cancer drug testing [13], respectively. 3D models have been employed as a platform for drug testing because they can recapitulate cell–cell and cell-ECM interaction and tissue mechanical properties [15, 21]. These 3D spheroid models have been used for

evaluations of drug sensitivity and resistance [34, 40]. Also, 3D models were applied to investigate effect of microenvironmental factors such as oxygen tension and nutrient consumption in 3D structure on the mechanism of drug or gene delivery [22]. There are several advantages of spheroids as a platform for drug/gene delivery testing. First, 3D spheroids can mimic 3D tissue architecture so that they can be used to better predict the performance of the delivery system *in vivo* than in 2D monolayer cells. This is because 3D spheroid model includes cell-cell and cell-ECM interaction as well as the diffusional limitation observed *in vivo*. Moreover, 3D spheroid models can mimic characteristic spatial distribution of cells in the solid tumor having central necrosis and hypoxia in their core, which is important for testing the anti-cancer drugs or gene delivery in these areas [33]. Compared to the wide application of 3D spheroids for testing chemotherapeutic drugs and stem cell regeneration [6, 42], there are less studies on the gene delivery research in 3D spheroid model except few reporting the physical electroporation transfection [29, 43] and the oligonucleotide delivery [5].

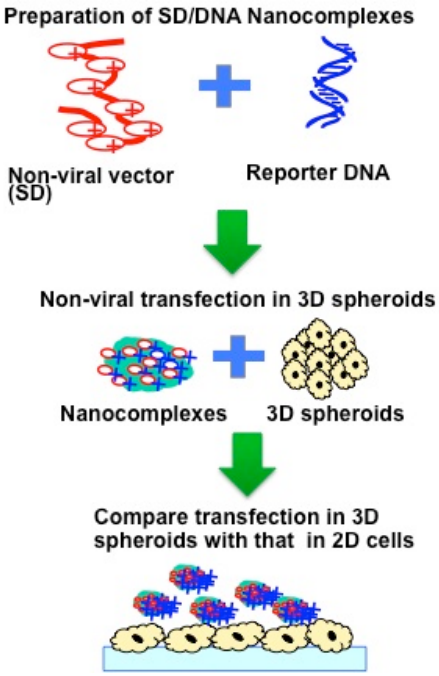

Figure 1. Schematic showing fabrication of non-viral nanocomplexes and their transfection efficiency tested in 2D *vs* 3D multicellular spheroids

The aim of this study was to increase our understanding of the transfection process of non-viral gene delivery vectors in a 3D spheroid model (Figure 1). Thus, our strategy was to construct uniform size 3D spheroids using HeLa cells and our novel polydimethyl siloxane (PDMS) micro-array technique. We also synthesized spermine-conjugated-dextran (SD) as a non-viral vector for the gene delivery into 3D spheroids. Then, cytotoxicity and transfection behavior of SD were compared with most widely used non-viral vector, branched polyethyleneimine (PEI, 25 kDa) in both conventional 2D monolayer cells and 3D spheroids. Finally, we compared the cellular uptake of the fluorescently labeled SD in 2D cells and 3D spheroids to investigate the possible mechanism that resulted in the differential transfection efficiency. Our study helps understanding the transfection process of non-viral gene delivery system in 3D spheroids, which is critical for the improvement and advancement of this therapeutic strategy. Also, this 3D spheroid model may be more relevant to *in vivo* setting and

may provide a useful high throughput *in vitro* screening platform for the novel non-viral gene delivery system in the future.

2.0 MATERIALS AND METHODS

2.1 Materials and Cells

All the chemicals were purchased from Sigma-Aldrich (USA) unless mentioned otherwise. Cell culture media, DMEM (Dulbecco's Modified Eagle Medium, 1X with 4.5g/L glucose, L-Glut and Sodium pyruvate), Dulbecco's phosphate buffered saline (DPBS) and serum were purchased from Mediatech Inc. (Manassas, USA). HeLa cell line and pLG2-Luc reporter plasmid were kindly provided by Dr. Song Li (School of Pharmacy, University of Pittsburgh, PA). HeLa cells were cultured in DMEM containing 10% fetal bovine serum (FBS, Hyclone, USA) under sterile conditions and maintained in 5% CO_2 at 37°C in a humidified incubator. RIPA (Radio-Immunoprecipitation Assay) buffer used for cell lysis samples in western blot was prepared using Tris (50 mM), pH 7.4, NaCl (150 mM), 0.5% sodium deoxycholate, 1% NP-40, 0.05 mM PMSF and protease inhibitor cocktail. Propidium iodide (PI) was purchased from Immunochemistry Technologies, LLC (USA). Hoechst 33342 was obtained from Thermo Fisher (USA). An enhanced green fluorescent protein plasmid (pcDNA3-EGFP, #13031) was purchased from Addgene (USA). It was propagated in *Escherichia coli* (*E. coli*) and isolated using DNA purification kit, GeneJET Plasmid Maxiprep Kit (Thermo Fisher, USA) as per the manufacturer's protocol.

2.2 Synthesis of Spermine-Conjugated Dextran (SD)

SD was synthesized according to previous report with slight modification [7]. Briefly, dextran (50 mg, M_w 70,000) was dissolved in 5 mL dimethyl sulfoxide (DMSO) followed by addition of 450 mg of carbonyldiimidazole (CDI) (molar ratio [CDI] / [OH] = 3) to activate the dextran. The activated dextran was then gradually added to 45 mL DMSO containing 1873.5 mg spermine with constant stirring and the reaction was continued for 24 h at room temperature. The crude product was dialyzed (*MWCO* 12-14 kDa) against ultrapure water for 48 h and lyophilized for 3 days to get the purified SD. The synthesis of SD was confirmed by Fourier transform infrared (FTIR) spectroscopy and proton nuclear magnetic resonance (^{1}H-NMR) spectroscopy. For FTIR, the spectra were recorded in absorption mode with a resolution of 4 cm^{-1} using FTIR spectrometer (Bruker Vertex 70, USA) with attenuated total reflection (ATR) attachment at a frequency range of 4000-600 cm^{-1}. For ^{1}H-NMR, the polymer samples were dissolved in $CDCl_3$ and the spectra were recorded by a NMR (Bruker 400, USA) at 400 MHz. Rhodamine-labeled SD (RSD) was also synthesized by conjugating spermine with Rhodamine-labeled dextran (M_w 70,000 Sigma-Aldrich, USA) according to the above mentioned procedure.

2.3 Preparation and Characterization of SD/DNA Nanocomplexes

The SD/DNA nanocomplexes were freshly prepared by complex coacervation method. Complexes were prepared by adding equal volumes of diluted SD solution and pDNA solution at different N/P ratios (nitrogen to phosphate ratio) followed by vortexing for 20 sec and incubation at room temperature for 15 min. The DNA complexation capability of SD was confirmed by

agarose gel electrophoresis. SD/DNA complexes at different N/P ratios (1:1, 2:1, 3:1, 4:1, 5:1 and 10:1) containing 0.5 µg DNA in each N/P ratio were loaded in 1% agarose gel having ethidium bromide as DNA visualizer. The gel was run in 1X TAE running buffer at 100 V for 30 min and subsequently the gel image was captured by gel documentation system (Gel Doc™ EZ System, USA). The particle size (hydrodynamic diameter) of SD/DNA complexes was measured by dynamic light scattering (DLS) using a Malvern Zetasizer (Zetasizer 3000, Malvern, USA). Prior to measurement, SD/DNA complexes were freshly prepared at different N/P ratios of 1:1, 2:1, 3:1, 4:1, 5:1, 10:1 and 20:1 as described above. The zeta potential of all complexes was also measured using the same instrument.

2.4 Fabrication of Polydimethyl Siloxane (PDMS) Stamps Containing Micropillar Arrays

PDMS stamps were fabricated using silicon master containing microwell arrays of diameters 300 µm as described previously [26]. Briefly, a mixture of pre-polymer silicone elastomer base solution and curing agent (Sylgard 184, Dow Corning Corporation, Midland, MI) at volume ratio of 10:1 was degassed for 10 min in a vacuum chamber to remove any bubbles and then poured onto the silicon master patterned with a SU-8 photoresist. It was further cured at 75°C for 45 min. PDMS stamps containing the micropillars were peeled from the masters.

2.5 Fabrication of Hydrogel Microwell Arrays

The generated PDMS stamps were subsequently used for fabrication of non-adhesive polyethylene glycol dimethacrylate (PEGDMA) microwell arrays on a glass slide. For covalent attachment of PEG hydrogel microwells to the glass slide, sodium hydroxide-treated glass slides were coated with 3-trimethoxysilyl polymethacrylate (TMSPMA) [23]. A micropillar PDMS stamp was placed on an evenly distributed PEGDMA 1000 (Sigma-Aldrich, USA) solution containing 1% (w/w) photoinitiator Irgacure-1959 (Ciba AG CH-4002, Basel, Switzerland) on the glass slide and then photocrosslinked by exposure to UV light (350–500 nm wavelength, 5W/cm^2) for 45 s using the OmniCure Series 2000 curing station (EXFO, Canada). After photocrosslinking of PEGDMA, the PDMS stamp was peeled from the substrate. This led to fabrication of 2×2 cm^2 device of hydrogel microwell arrays.

2.6 Generation and Characterization of 3D Multicellular Spheroids

Microwell arrays (2×2 cm^2) with a well size of 300 μm were sterilized in 6-well plates using 70% isopropanol under UV light for 30 min and washed with DPBS three times. HeLa cell suspension (100 μL, 1×10^7 cells/mL) was seeded onto each array and cells were allowed to settle in the microwells by gravity for 30 min. This step was repeated one more time to ensure complete filling of the microwells. The microwell array was then washed gently three times with DPBS to remove undocked cells. The cell-seeded devices were cultured in DMEM with 10% FBS in humidified incubator at 37°C. The culture media was changed every day.

To evaluate the spatial cell distribution in the 3D spheroids, spheroids were stained by Ki-67 (proliferation marker)/PI (cell death marker). 3D HeLa spheroids grown in 300 μm size microwells were harvested on day 2. Spheroids were incubated with PI (1:1000) diluted in growth media inside the CO_2 incubator for 2 h. Subsequently, they were washed and fixed with 4% paraformaldehyde for 20 min followed by washing with DPBS three times. Spheroids were further fixed with 95% methanol on ice for 15 min and permeabilized by 0.1% TritonX-100 (in 3% BSA) for 1 h. Then, they were stained with primary antibody Ki-67 (H-300) (Santa Cruz, USA, 1:100) diluted in 3% BSA by incubation at 4°C overnight. After washing with DPBS three times, the spheroids were stained with Alexa-Fluor conjugated anti-rabbit secondary antibody (Santa Cruz, USA, 1:500) for 1 h at room temperature.

2.7 Evaluation of The Transfection of SD/DNA on 2D Monolayer Cells and 3D Spheroids

For *in vitro* transfection in 2D monolayer cells and 3D spheroids, both luciferase and GFP plasmid DNA (pDNA) were used. Before transfection, 1×10^5 HeLa cells or 20 spheroids were seeded on 24 well plates and cultured for 24 h in complete media. Freshly prepared SD/DNA nanocomplexes at different N/P ratios (1:1, 2:1, 3:1, 4:1, 5:1 and 10:1) containing 1 μg DNA in each ratio were added to the cells in serum-free media. After incubation for 4 h, the transfection media was replaced with fresh 10% FBS containing media and further incubated for 20 h in 5% CO_2 incubator at 37°C. Naked pDNA and PEI/DNA complex (N/P ratio 10:1) were used as negative and positive control, respectively. After 24 h transfection, the luciferase activity was assayed by luminescence spectrophotometer and the EGFP (enhanced green fluorescence

protein) expression of transfected cells was observed by confocal laser scanning microscopy (FV1000, Olympus) or western blot.

For confocal observation, the transfected 2D cells were fixed by 4% paraformaldehyde followed by nuclear staining with Hoechst at room temperature for 30 min while the transfected 3D spheroids were fixed followed by nuclear staining with Hoechst at 4 °C overnight. The GFP expression was further determined by western blot assay according to the standard protocol. The transfected cells were first lysed by RIPA buffer on ice for 1 h and the western blot assay was carried out after treating the cell lysate with different antibodies including anti-EGFP-TAG mouse primary antibody (Thermo Scientific, USA), anti-beta-actin mouse primary antibody (Thermo Scientific, USA) and the Dylight 680 fluorescently labeled Goat Anti-mouse as secondary antibody (Thermo Scientific, USA). For luciferase expression, pGL2-Luc transfected cells were lysed. Then, the luciferase expression for each group was assayed by Pierce Firefly Luc One-step Glow Assay Kit (Thermo Scientific, USA). Induction was normalized to protein concentration determined by a Commassie (Bradford) Kit (Thermo Scientific, USA).

2.8 *In Vitro* Cytotoxicity Assay

For viability assay, 1×10^5 cells HeLa cells or 20 spheroids were seeded into 24-well plate and cultured for 24 h in complete media. Freshly prepared SD/DNA nanocomplexes at different N/P ratios (1:1, 2:1, 3:1, 4:1, 5:1 and 10:1) containing 1 μg DNA in each ratio were added to the cells with serum-free media. After incubation for 4 h, the transfection medium was replaced with fresh 10% FBS containing medium and further incubated for 20 h in 5% CO_2 incubator at 37°C. Naked pDNA and PEI/DNA complex (N/P ratio 10:1) were used as negative and positive

control, respectively. After 24 h transfection, the old culture media was replaced by 10% alamarBlue® Cell Viability Assay solution (Thermo Scientific, USA) in complete DMEM media (containing 10% FBS). After 4 h incubation, the OD value at 595 nm of each well was measured by microplate spectrophotometer (Biotek, USA). All experiments were repeated at least three times with at least 3 replicates to ascertain reproducibility.

2.9 Comparison of Cellular Uptake of SD/DNA Complex on 2D Monolayer Cells and 3D Spheroids

The cellular uptake of Rhodamine-conjugated SD (RSD) polymer and RSD/DNA complex at N/P ratios of 3:1 and 5:1 was carried out in 2D monolayer cells and 3D spheroids. Before cellular uptake study, the RSD/DNA complexes were freshly prepared as discussed above and the complexes containing 1 μg DNA in each weight ratio were added to the cells in serum free media followed by incubation in CO_2 incubator at 37 °C for 4 h. The 2D cells and 3D spheroids were fixed by 4% paraformaldehyde for 20 min followed by nuclear staining with Hoechst. The cells were then imaged by confocal microscopy. The images were obtained as a Z-stack with a step size of 5 microns using 40X objective.

2.10 Statistics

Cell viability, luciferase activity and quantified western blot data was expressed as means ± SEM and the data of characterization of nanocomplexes and spheroids was expressed as means ± SD.

Student’s paired t-test was used for comparisons between two groups. Multiple comparisons were done using one-way/two-way ANOVA followed by Tukey's post hoc test (OriginPro8 SRO v. 8.07). *p*-values less than 0.05 was considered significant.

3.0 RESULTS AND DISCUSSION

3.1 Characterization of SD

For successful gene therapy, the gene carrier should show efficient transfection and be safe. To achieve this, we first synthesized dextran-based gene delivery vector through conjugating cationic spermine as shown in Figure 2A. There are different methods to conjugate the cationic spermine to polysaccharide dextran backbone [1]. The conjugation using CDI is one of the most convenient method [17]. To avoid any crosslinking, excess amount spermine was used to react with dextran through CDI. The synthesis of SD was characterized by ^{1}H-NMR (Figure 2B), FTIR (Figure 2C) and elemental analysis (Figure 2D).

The ^{1}H-NMR spectra showed the characteristic peaks of spermine at 1.5, 1.6-1.7 and 2.5-2.7 ppm [41]. Dextran showed the characteristic peaks at 3.5-3.7, 3.7-3.85, 3.9-4.1 and 5 ppm [36]. After conjugation of spermine with dextran, the appearance of proton peaks of spermine at 1.5-2.0 ppm along with the characteristic peaks of dextran indicated successful synthesis of SD. The FTIR spectra (Figure 2C) showed the typical absorbance peaks of spermine at 3255 cm^{-1} (N-H stretching of primary amine) and 1647 cm^{-1} (N-H bending of primary amine). Dextran showed a broad peak at 3440 cm^{-1} corresponding to the hydrogen bonded O-H stretching of hydroxyl groups. After reaction of spermine with dextran through CDI, the appearance of absorbance peak

at 1738 cm^{-1} corresponding to C=O stretching of carbamate group (-NH-CO-O), further providing the evidence of the synthesis of SD.

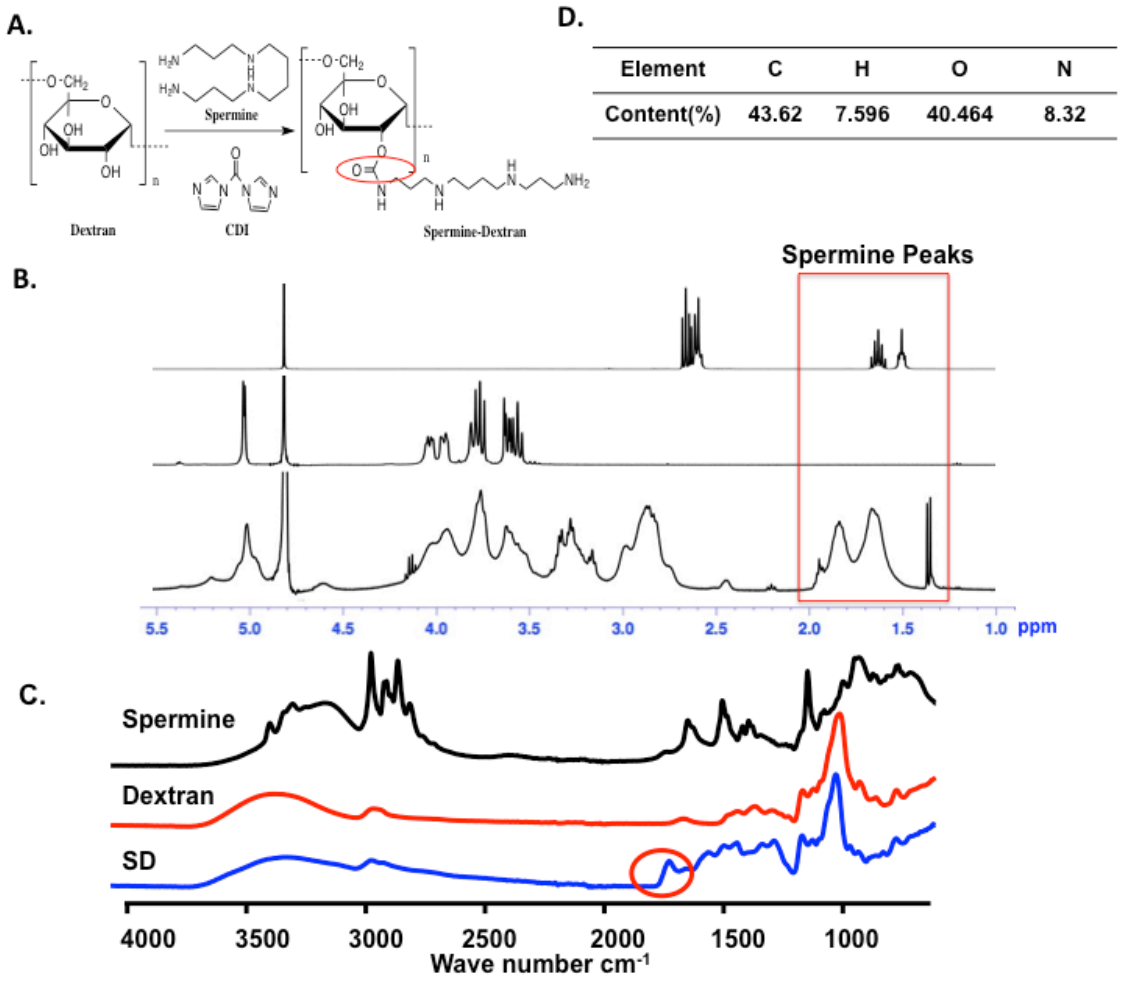

Figure 2. Synthetic route of SD and Characterization of SD

A. Synthetic schema of SD; B. ^{1}H-NMR spectra of spermine, dextran and SD; C. FTIR spectra of spermine, dextran and SD; The peak at 1738 cm^{-1} corresponds to C=O stretching of carbamate group (-NH-CO-O); D. Elemental Analysis of SD.

The synthesized product was also characterized by elemental analysis (Department of Chemistry, Zhejiang University, China) as shown in Figure 2D. From ^{1}H-NMR results, the theoretical nitrogen percentage of SD was 7.5% while the actual nitrogen percentage in SD determined from elemental analysis was 8.32%. This is helpful to calculate the N/P ratio of

SD/DNA during complex formation [7]. The N/P ratio is more reliable parameter compared to weight ratio because the N/P ratio is directly related to the positive charge of polymer and the negative charge of DNA as the nanocomplexes are formed through ionic interactions between phosphate and amine of DNA and polymer, respectively.

3.2 Characterization of SD/DNA Nanocomplexes

SD/DNA nanocomplexes were formed by self-assembled complex coacervation method through electrostatic interactions of negatively charged pDNA with positively charged SD polymer [20]. The complex formation was confirmed by agarose gel electrophoresis as shown in Figure 3A. The plasmid DNA was only partly condensed by SD at lower N/P ratio (1:1) through ionic interactions, which suggested that the complexation capability of SD is not enough to compact all DNA at this ratio. With the increase of N/P ratio, the migration of DNA was completely retarded when the N/P ratio was more than 3:1, which indicates the complete complexation of all DNA by SD.

Since the hydrodynamic size and surface charge of nanocarriers are very important for drug and gene delivery, the average particle size and z-potential of the SD/DNA complexes were determined by dynamic light scattering (DLS). In Figure 3B, it can be seen that the average particle size of SD/DNA complexes decreased gradually with increase in N/P ratio. At low N/P ratio (1:1), the particle size was higher (97.1 ± 13.6 nm) due to incomplete complexation of DNA with SD. The particle size and morphology of SD/DNA complex at N/P ratio 3:1 were further characterized by TEM as shown in Figure 3B. TEM image also showed that the particle sizes of SD/DNA complexes were around 45-65 nm with some aggregates, which were well

correlated to the DLS data. The particle size determined by DLS was slightly higher than that of the TEM image because DLS measurement carried out in aqueous media. The morphology of the complex was spherical in shape.

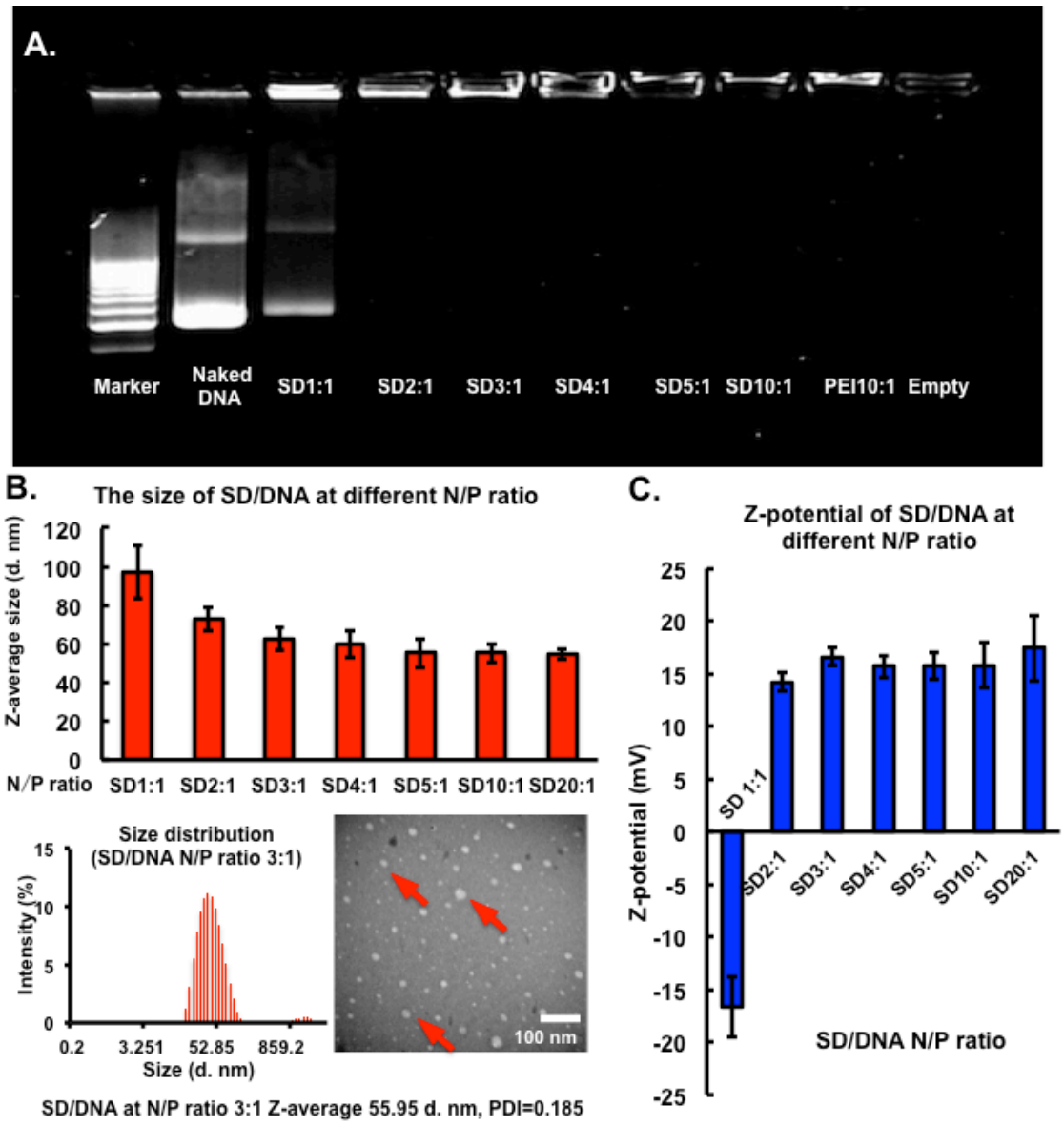

Figure 3. Characterization of SD/DNA nanocomplexes

A. Agarose gel electrophoresis of SD/DNA nanocomplexes; B. Size of SD/DNA nanocomplexes at different N/P ratios and size distribution and TEM of SD/DNA nanocomplexes at N/P ratio 3:1; C. zeta-potential of SD/DNA nanocomplexes at different N/P ratios. The results were expressed as means ± SD.

Zeta potential is an important parameter for cellular uptake. Positive zeta potential is reported to favor cellular uptake because cell membrane possesses negative charge, which facilitate better cellular uptake of positively charged particle through electrostatic interaction. The zeta potential of SD/DNA nanocomplexes at different N/P ratio was shown in the Figure 3C. At N/P ratio 1:1 was negative because the excessive negative DNA could not be fully condensed by positive SD. When N/P ratio reached to 2:1, the zeta potential of nanocomplexes became positive and remained almost constant with increase in N/P ratio of SD/DNA complex due to complexation of pDNA by SD as observed in agarose gel electrophoresis assay. This positive charge can help the SD/DNA nanocomplexes interact with the negatively charged cellular membrane and enhance the cellular internalization and transfection efficiency of the nanocomplexes [24]. Additionally, the proton sponge effect of spermine has been shown to increase transfection efficiency [9]. The high degree of protonation makes it easier for the DNA to escape from the endosome and be trafficked through the cytoplasm to the nucleus for gene expression. Also, the positive charge of the SD/DNA nanocomplexes would improve the cell-carrier interaction and cellular uptake of nanocomplexes.

3.3 Transfection and Cytotoxicity of SD/DNA Nanocomplexes on 2D Monolayer Cells

Safety is one of the most important concerns for the application of the non-viral gene delivery vehicles. The toxicity of SD/DNA nancomplexes at different weight ratios was investigated by an alamarBlue® Cell Viability Assay. Branched PEI (25 kDa)/pDNA complex at N/P ratio 10:1 was used as positive control because branched PEI (25 kDa) is most widely used non-viral carrier with high transfection efficiency at N/P ratio 10:1. [16, 32]. From the cell viability assay

as shown in Figure 4A, it was found that the commercial reagent PEI (25 kDa) showed high cytotoxicity, which agreed with most of the non-viral gene delivery studies [18, 37]. SD/DNA complexes showed dose-dependent cytotoxicity on 2D monolayer cells. The cell viability was >80% for 2D cells at low N/P ratio (N/P ratio from 1:1 to 4:1), which was much lower than that of positive control PEI/pDNA complexes. However, SD/DNA complexes showed comparable toxicity to PEI at higher N/P ratio (10:1). The high cytotoxicity of SD/DNA at N/P ratio 10:1 may be due to their high positive charge [44], which can cause cell membrane damage. Also, it was reported that the cationic polymers with the primary amine could interfere with critical intracellular processes of cells [11].

The transfection efficiency of SD/DNA nanocomplexes were investigated by luciferase activity assay, confocal fluorescence observation and western blot technique. The levels of luciferase activity (RLU/mg protein) were obtained following transfection with a range of SD/DNA at N/P ratio from 1:1 to 10:1 (Figure 4B). The luciferase activity increased with increase in N/P ratio of SD/DNA complex up to 3:1 then the luciferase activity slightly decreased with further augmentation of N/P ratio. The luciferase activity obtained by SD/DNA complex at N/P ratio 3:1 was almost comparable to that of PEI at N/P ratio 10:1. There was no significant difference between PEI group and SD N/P ratio 3:1 and 5:1 group (p>0.05). At lower N/P ratio (1:1 and 2:1), the transfection efficiency was lower than PEI/DNA nanocomplexes. This may be because the SD polymer cannot fully condense the plasmid DNA to form nanocomplexes with positive charge and small size (Figure 3A, B and C). From N/P ratio 3:1 to N/P ratio 5:1, the well-formed SD/DNA nanocomplexes have good DNA complexation properties and showed good transfection behavior. However, at higher N/P ratio (N/P=10:1), the transfection efficiency decreased significantly compared to PEI as well as SD/DNA

nanocomplexes at 3:1-5:1 ratios. This might be due to the significant cytotoxicity of the excessive positive charges on SD (Figure 4A).

The luciferase assay method is very sensitive but sometimes the quenching of firefly luciferase-luciferin bioluminescence would influence the transfection results. Also, the above data has reported the total reporter gene in HeLa cells, but do not indicate the proportion of cells transfected or the localization of gene delivery vector in the cells. To address these issues, the reporter gene was switched to pcDNA3-EGFP to investigate the localization of reporter EGFP expression in 2D monolayer cells using confocal microscopy. Figure 4C showed EGFP expression in 2D HeLa cells after transfection with pcDNA3-EGFP delivered by SD and PEI as delivery vectors. The green fluorescence protein signal was weaker in HeLa cells transfected by naked DNA and SD/DNA complexes with low N/P ratio (1:1). However, stronger fluorescent intensity was observed when 2D cell were transfected by SD/DNA with N/P ratio 3:1 and 5:1. This result indicates that the SD/DNA nanocomplexes internalized into cytoplasm followed by GFP expression.

For successful gene therapy, the efficacy of therapeutic gene expression not only depends on the gene transfection signal but also on the amount of protein expression. To further confirm EGFP protein expression after transfection in 2D cells, we performed western blot assay as shown in Figure 4D. The relative amount of each immunoprecipitated protein was quantified with ImageJ software. The results showed that the EGFP expression of SD/DNA complex increased with increase in N/P ratio. SD/DNA complex at N/P ratio of 3:1 and 5:1 groups showed the highest EGFP expression which was almost equivalent to PEI group and the result correlated well with the luciferase assay and confocal observation.

Therefore, SD/DNA complex at N/P ratio of 3:1 and 5:1 showed good transfection efficiency (almost equal to that of PEI/DNA) with minimal toxicity (much less than PEI/DNA). It is already reported that dextran is biocompatible, biodegradable and nontoxic polysaccharide with low transfection efficiency due to non-ionic nature [10, 19]. Conjugation of cationic spermine with dextran also resulted in low toxicity and efficient gene delivery in 2D cells.

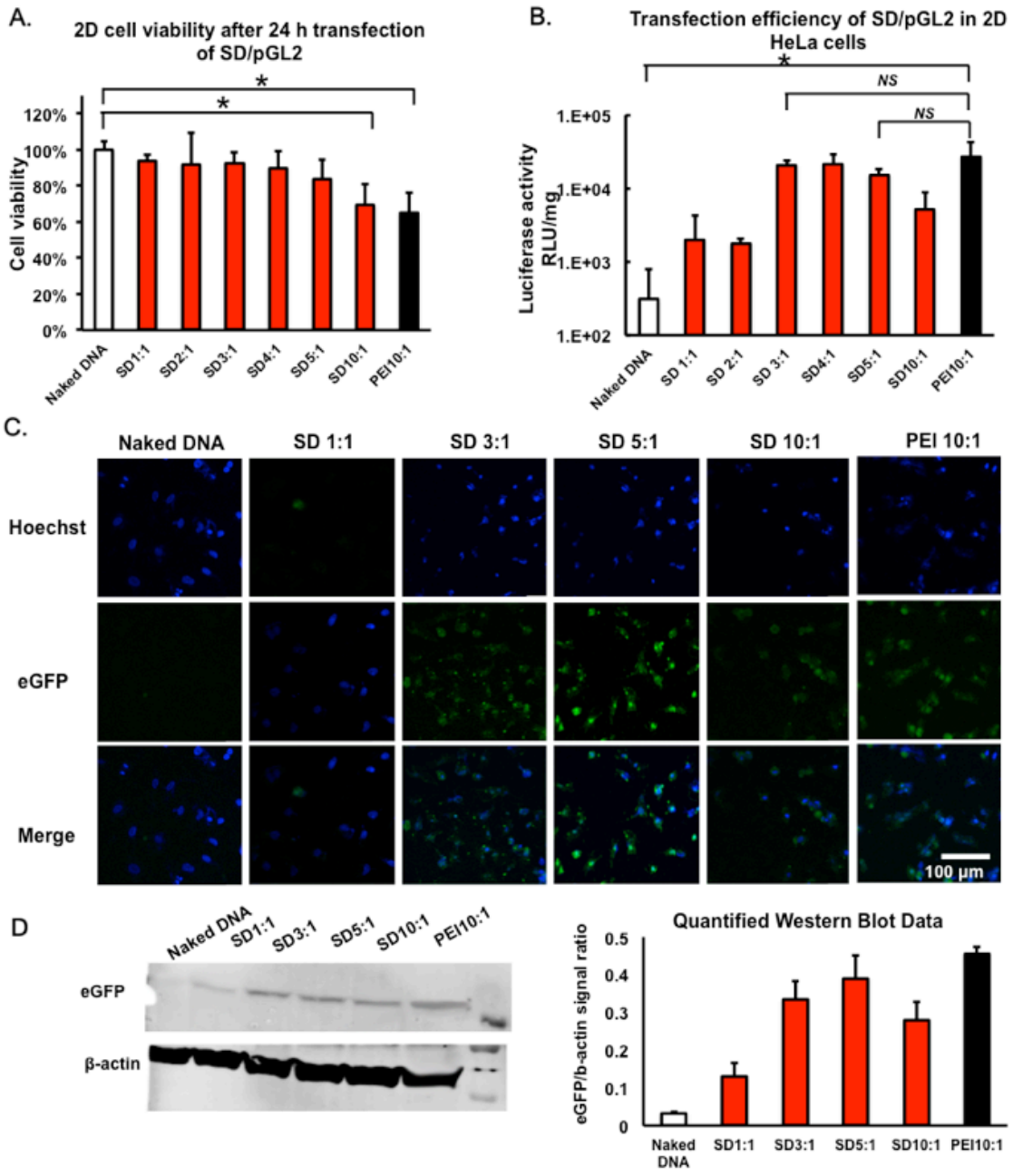

Figure 4. Cytotoxicity and transfection efficiency of SD/DNA nanocomplexes in 2D monolayer HeLa cells A. Cell viability of 2D monolayer cells after transfection with SD/DNA and PEI/DNA nanocomplexes at different N/P ratioa; B. Luciferase activity after 24 h SD/pGL2 nanocomplexes transfection at different N/P ratios. *NS*, no significant difference; * significant difference (One-way ANOVA, $p<0.05$); C. Confocal images of 2D monolayer HeLa after 24 h SD/pEGFP nanocomplexes transfection at different N/P ratios. Top panels: Hoechst nuclear stain (blue); middle panels: EGFP expression (green); bottom panels: Merged

images; D. Western blot of EGFP from 2D monolayer HeLa after 24 h transfection with SD/pEGFP nanocomplexes at different N/P ratios and optical density quantification of EGFP/b-actin by the ImageJ software. The results were expressed as means ± SEM.

3.4 Characterization of 3D Spheroids

Several studies utilized different techniques and methods to form 3D spheroids for drug screening and other biological studies. Some of them cannot maintain intact 3D structure due to less stability and resulted in failure of drug screening study [39]. Some other conventional techniques such as Non-adherent surfaces, Spinner flask and NASA rotary cell vessel culture techniques cannot fabricate 3D spheroids with uniform and controlled sizes [13, 22]. Size uniformity is very important because spheroids with different sizes may have different physical and biological properties such as presence of hypoxia, metabolic stress due to nutrient/metabolite diffusion limitations. Non-uniform size of spheroids may also influence the experimental reproducibility by affecting penetration of drug or gene delivery vectors. To overcome these problems, we developed a simple multilayer replica molding technique to prepare intact 3D spheroids with uniform and controlled sizes. In our study, polydimethyl siloxane (PDMS) and polyethylene glycol dimethacrylate (PEGDMA) were serially replica molded to develop hydrogel device (Figure 5A). PDMS micro-array is widely used for microfluidic and nano-imprint lithography and few studies have utilized it for fabricating hydrogel microwell devices for cancer spheroids and stem cell embryoid bodies [28].

Our technique could produce hundreds of spheroids with uniform size (250 ± 28 μm) from one PEGDMA gel device in a high throughput manner (each 2×2 cm^2 device contained

approximately 625 spheroids of 300 μm sizes) (Figure 5B, C). The 2-day old spheroids were harvested by pipetting and most of them remained intact and tight (Figure 5C, E). After dissociation into single cell suspension by trypsin treatment, the average number of cells in each harvested spheroid was around to be 1143 ± 110.

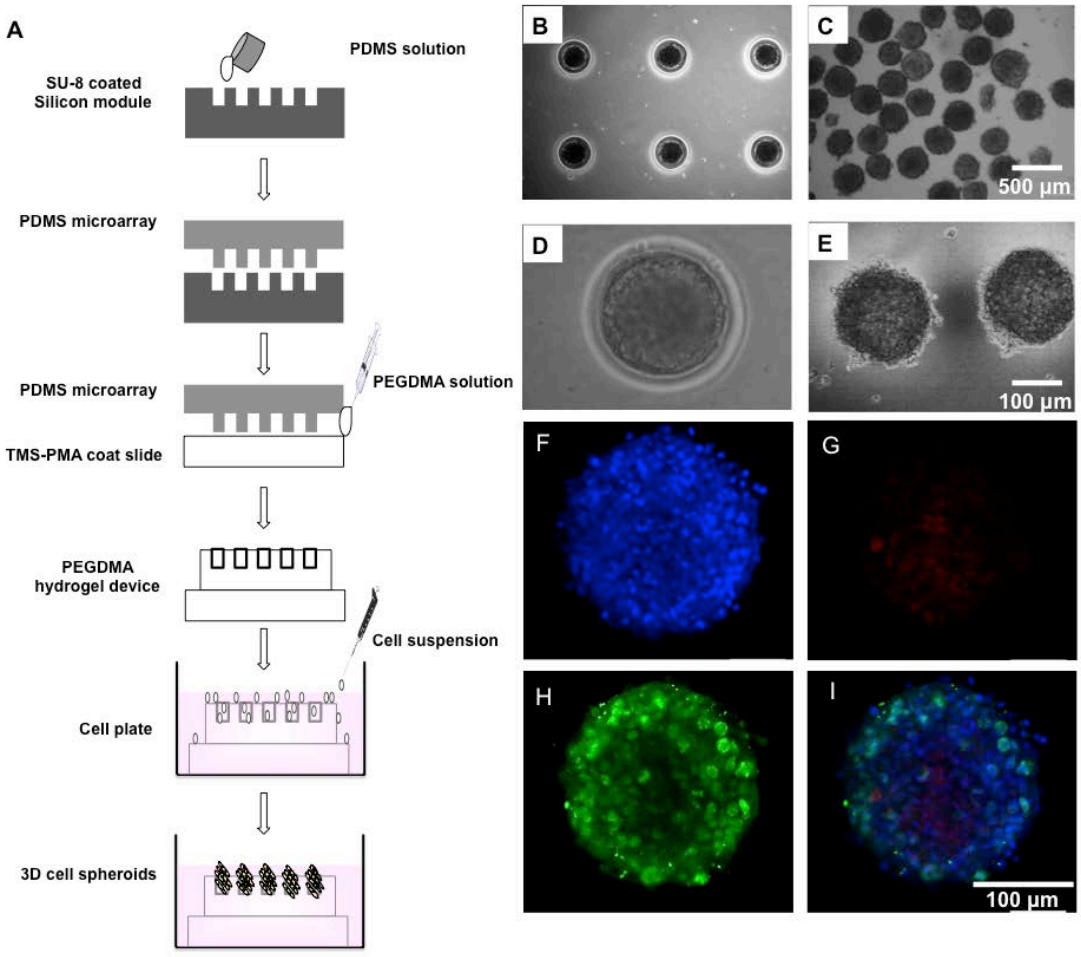

Figure 5. Fabrication and characterization of 3D spheroids

A. Schematic of fabrication of 3D spheroids using PDMS and PEGDMA hydrogel; B. Uniform spheroids cultured in hydrogel device; C, E. 2-day old harvested spheroids; D. Single spheroid in a hydrogel microwell; F. Hoechst nuclear stain; G.PI Dead cell stain; H. Ki67 marker stain; I. Merged images.

To assess the spatial cellular distribution of proliferating and apoptotic cells in the spheroids, Ki67 immunostaining was performed. Ki67 protein is present during all active cell phase including G1, S, G2, and mitosis except resting cell G0 phase [35]. This property makes it an excellent marker for proliferating cellular population [14]. It is reported that spheroids with diameter of 400 μm and larger size would have zones of proliferating cells on the outside and quiescent cells on the inside due to nutrient and oxygen transport limitations [40]. However, in this study, we used spheroids with smaller sizes (250 ± 28 μm) that were harvested on day 2. As shown in Figure 5F, 3D spheroids exhibited Ki67-positive cells with few PI-positive (dead) cells in the central core of the spheroids (Figure 5G). Based on these observations, HeLa cells can form uniform 3D spheroids in our PEGDMA-device system and these spheroids can be further employed as the avascular microtumor model for studying drug and gene delivery efficiency.

3.5 Evaluation of The Transfection and Cytotoxicity of SD/DNA Complexes in 3D Spheroids

The gene transfection efficiency and cytotoxicity of SD/DNA complex at different N/P ratios was evaluated in 3D spheroids as shown in Figure 6. To compare the difference of the cytotoxicity of the polymeric nanocomplexes in 3D spheroids, an alamarBlue® cell viability assay was performed. Figure 6A showed the cell viability after 24 h transfection in 3D spheroids. There was no significant difference in cell viability in 3D spheroids transfected by SD/DNA complexes at all N/P ratios and PEI. In 3D spheroids, SD/DNA complexes at N/P ratios of 3:1 and 5:1 showed higher cell viability, which was similar to that observed in 2D cells. The higher N/P ratio of SD/DNA complex (10:1) and PEI/DNA complex showed higher cytotoxicity as well

as transfection efficiency in 2D cells especially for PEI. However, this trend was not observed in 3D spheroids.

Figure 6B showed that the overall luciferase activity was very low (10 fold lower than that on 2D cells). And there was no significant difference in the luciferase expression among different N/P ratios of SD/DNA nanocomplexes and PEI. Since N/P ratio dependent transfection was obtained in 2D monolayer cells, it was expected that the same trend would be obtained in the 3D spheroids. However, we didn't see such results in 3D model. The SD/DNA complex at N/P ratio 3:1 to 10:1 showed the similar efficiency as the naked DNA suggesting that the SD/DNA nanocomplexes induced low transfection in 3D spheroids without any dose-dependent behavior.

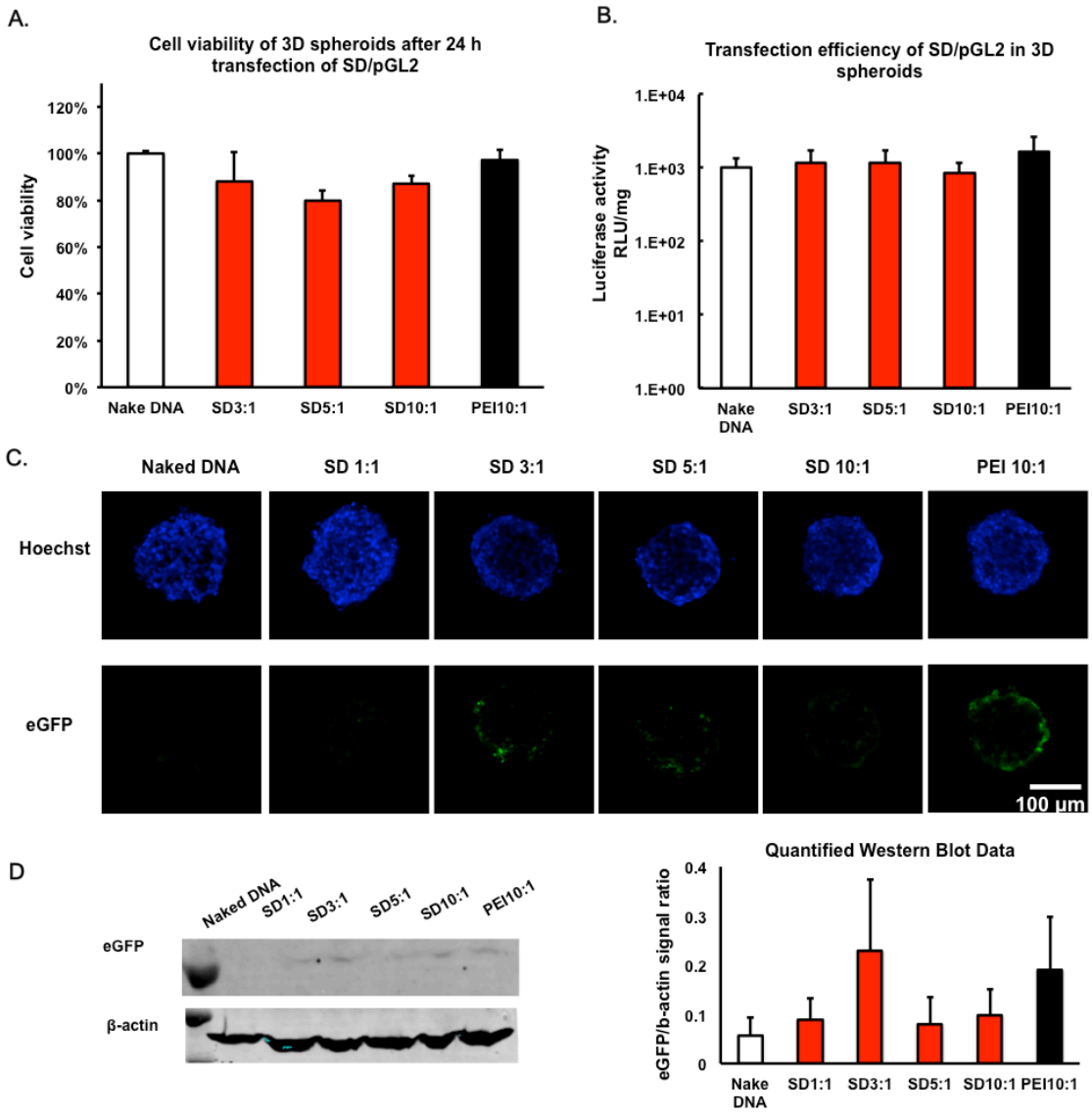

Figure 6. Cytotoxicity and transfection efficiency of SD/DNA nanocomplexes in 3D spheroids

A. Cell viability of 3D spheroids after 24 h SD/pGL2 nanocomplexes transfection at different N/P ratios; B. Luciferase activity after 24 h SD/pGL2 nanocomplexes transfection at different N/P ratios. C. Confocal images of 3D spheroids after 24 h SD/pEGFP nanocomplexes transfection at different N/P ratios. Top panels: Hoechst nuclear stain (blue); bottom panels: EGFP expression (green); D. Western blot of EGFP expression after 24 h transfection with SD/pEGFP nanocomplexes at different N/P ratios and optical density quantification of EGFP/b-actin by the ImageJ software. The results were expressed as means ± SEM.

We also observed the transfection efficiency of these polymeric vectors in 3D spheroids by confocal microscopy. In Figure 6C, it can be observed that the EGFP expression of the transfected cells by SD/DNA and PEI/DNA complexes at all N/P ratios were much lower than that on 2D cells. It was reported that EGFP expression was confined to the outermost 3–5 cell layers in some other spheroids, but most of the proportion of cells expressing EGFP is less than 5% of the total population [31]. We obtained similar transfection in PEI/DNA group and SD/DNA ay N/P ratios of 3:1 and 5:1 groups, where it was observed that EGFP expression was limited to the peripheral cells of the spheroids. The western Blot (Figure 6D) also showed similar results as confocal results that PEI and SD/DNA at N/P ratio 3:1 and 5:1 exhibited less protein expression.

It is commonly known that the spheroids display extensive cell-cell contact, a concomitant elevation in the interstitial pressure and demonstrate a significant resistance to chemotherapy and radiotherapy [8]. This may also be true for the non-viral gene delivery systems. The extracellular matrix (ECM) and multicellular barriers with high cell density inhibited the nanocomplexes penetrating into the deep areas of 3D spheroids. Some other studies on gene delivery in 3D spheroids also showed similar low transfection efficiency in spheroids [4, 25, 30, 31]. Further experiments are required to confirm the diffusion and penetration barriers for non-viral vectors . It is a well-known dilemma that the transfection efficiency and cytotoxicity of non-viral gene delivery is closely related, which suggests that the higher transfection efficiency may be associated with higher cytotoxicity. In our study, we observed this phenomenon and demonstrated it was true for the transfection on both of 2D and 3D spheroids. Taken all of above transfection results together (luciferase assay, confocal fluorescence images and western blot

assay), SD demonstrated good transfection efficiency when tested in conventional 2D monolayer cells, while both of SD and PEI did not show high transfection efficiency in 3D spheroids. Only parts of the peripheral cells (outermost cell layers) in 3D spheroids were transfected by PEI/DNA and SD/DNA complexes (N/P ratio 3:1 and 5:1). These results are similar to the few published studies on *in vitro* 3D spheroid model for gene delivery [5] [31] and also suggested the possible relevant clinical observation that non-viral gene delivery has low efficiency in the solid tumors or 3D architectural tissues *in vivo*. These data suggests that the biological barriers present in 3D tissue structure serve as a major obstacle to block the penetration of non-viral gene delivery vector into the 3D tissues, thus further hampering gene delivery and transfection efficiency. To further test the penetration of SD and PEI vectors, we compared the cellular uptake of these vectors in both 2D monolayer cell and 3D spheroids.

3.6 Evaluation of The Cellular Uptake of Rhodamine-conjugated Spermine-Dextran (RSD) in 2D Cells and 3D Spheroids

Above transfection results showed that the transfection efficiency of SD/DNA (N/P ratio 3:1 and 5:1) and PEI/DNA were less in 3D spheroids than that in 2D cells and most of the transfected cells in 3D spheroids were located at the outer layers. This result suggested that one of the reasons for this phenomenon may be due to their failure to penetrate in the 3D tissues [27, 38]. To further assess the penetration behavior of SD/DNA nanocomplexes in 3D cells, we used fluorescently-labeled SD, Rhodamine-conjugated Spermine-Dextran (RSD), to track the cellular uptake of the non-viral vector by using confocal microscopy. The RSD/DNA complexes at N/P ratios of 3:1 and 5:1 were used in cellular uptake study due to their best transfection efficiency in

2D cells and 3D spheroids. From Figure 7, it was observed that the cellular uptake of RSD/DNA nanocomplexes at N/P ratio of 3:1 and 5:1 (Figure 7B, C) was higher than free RSD in 2D monolayer (Figure 7A). However, the cellular uptake of the same was significantly lower in 3D spheroids compared to that in 2D monolayer cells and resulted in low transfection efficiency in 3D spheroids. The uptake of the RSD/DNA nanocomplexes by the cells in 3D spheroids could be depicted by the weak fluorescence signal in the peripheral layer of the 3D spheroids (Figure 7E, F). This suggested that the RSD/DNA nanocomplexes were only able to accumulate in cells at the exterior of the 3D spheroid and most of the non-viral vectors were blocked in the peripheral layers. This result also agreed with the transfection result in 3D spheroids (Figure 6C). The different internalization behavior between on 2D monolayer cells and 3D spheroids cells might be due to the biological barrier in 3D spheroids. This would largely influence the transfection and cytotoxicity behavior in the 2D cells and 3D spheroids. Future experiments concerning the different microenvironment and cellular trafficking in 3D spheroids should be done to further disclose the mechanism that induce the different transfection behavior of gene delivery system in 2D monolayer cells and 3D spheroids.

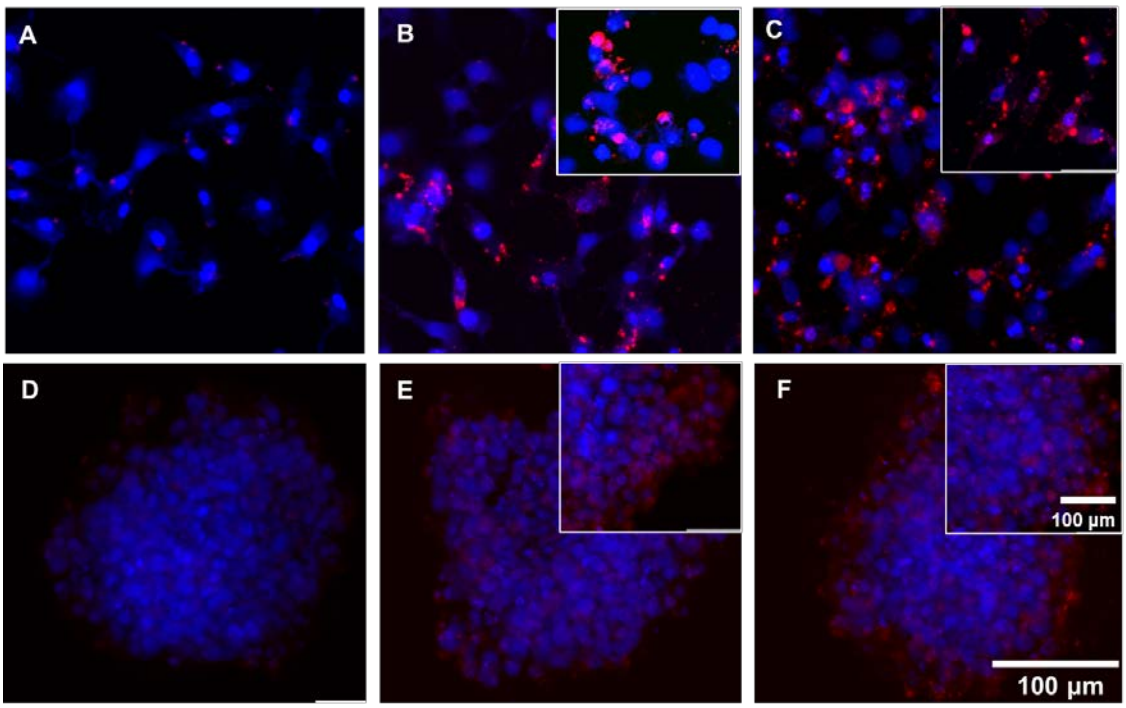

Figure 7. The cellular uptake of RSD/DNA nanocomplexes after 4 h incubation.

Cellular uptake of RSD polymer (A), RSD/DNA nanocomplexes at N/P ratio of 3:1 (B) and 5:1 (C) in 2D cell monolayers;

Cellular uptake of RSD polymer (D), RSD/DNA nanocomplexes at N/P ratio of 3:1 (E) and 5:1 (F) in 3D spheroids; Blue: Hoechst nuclear stain; Red: RSD/DNA nanocomplexes. Inset shows high magnification (80X) images. The images represent the central slice of the z-axis scan.

4.0 CONCLUSION AND FUTURE DIRECTION

The transfection efficiency of synthesized SD was compared in 2D monolayer cells and 3D spheroids. It was found that the transfection efficiency, cytotoxicity and cellular uptake of SD in 3D spheroids were much lower than in 2D cells. The possible reason might be the biological barriers and strong cell-cell interactions in 3D spheroids hindering the non-viral vectors penetration into the inner core of the spheroids. Although 3D spheroid model cannot fully resemble the *in vivo* 3D tissues and solid tumors a, they provide useful information of drug or gene delivery vector penetration in tissues and can better predict the *in vivo* behavior than 2D monolayer cell models. A follow-up study will investigate the detailed mechanisms behind the poor transfection in 3D and possible avenues to overcome these barriers. This work will refine the 3D drug and gene delivery system testing model and provide a promising platform for the drug and vector screening prior to the *in vivo* study.

APPENDIX A

ABBREVIATION

Term	Abbreviation
AGE	Agarose Gel Electrophoresis
ECM	Extracellular Matrix
EGFP	enhanced Green Fluorescence Protein
FTIR	Fourier Transform Infrared Spectroscopy
MCTS	Multicellular Tumor Spheroids
PBS	Phosphate Buffered Saline
PDMS	Poly-Dimethylsiloxane
PEGDMA	Poly-(Ethylene Glycol) Diamethacrylate
PEI	Poly-ethyleneimine
PFA	Poly-formaldehyde
PI	Prodium Iodide
RLU	Relative Light Unit
RSD	Rhodamine-labeled Spermine-Dextran
SD	Spermine-Dextran
TEM	Transmission Electron Microscopy

BIBLIOGRAPHY

[1] T. Azzam, H. Eliyahu, A. Makovitzki, M. Linial. A.J. Domb, Hydrophobized dextran-spermine conjugate as potential vector for in vitro gene transfection. *Journal of controlled release : official journal of the Controlled Release Society*, 96: 309-323, 2004.

[2] C. Baum, O. Kustikova, U. Modlich, Z. Li. B. Fehse, Mutagenesis and oncogenesis by chromosomal insertion of gene transfer vectors. *Human gene therapy*, 17: 253-263, 2006.

[3] N. Bessis, F.J. GarciaCozar. M.C. Boissier, Immune responses to gene therapy vectors: influence on vector function and effector mechanisms. *Gene therapy*, 11 Suppl 1: S10-17, 2004.

[4] P.J. Canatella, M.M. Black, D.M. Bonnichsen, C. McKenna. M.R. Prausnitz, Tissue electroporation: quantification and analysis of heterogeneous transport in multicellular environments. *Biophysical journal*, 86: 3260-3268, 2004.

[5] K. Carver, X. Ming. R.L. Juliano, Multicellular tumor spheroids as a model for assessing delivery of oligonucleotides in three dimensions. *Molecular therapy. Nucleic acids*, 3: e153, 2014.

[6] J.M. Cha, H. Bae, N. Sadr, S. Manoucheri, F. Edalat, K. Kim, S.B. Kim, I.K. Kwon, Y.-S. Hwang. A. Khademhosseini, Embryoid body size-mediated differential endodermal and mesodermal differentiation using polyethylene glycol (PEG) microwell array. *Macromolecular Research*, 23: 245-255, 2015.

[7] Y.Z. Chen, G.X. Ruan, X.L. Yao, L.M. Li, Y. Hu, Y. Tabata. J.Q. Gao, Co-transfection gene delivery of dendritic cells induced effective lymph node targeting and anti-tumor vaccination. *Pharmaceutical research*, 30: 1502-1512, 2013.

[8] B. Desoize. J. Jardillier, Multicellular resistance: a paradigm for clinical resistance? *Critical reviews in oncology/hematology*, 36: 193-207, 2000.

[9] H. Eliyahu, A. Joseph, T. Azzam, Y. Barenholz. A.J. Domb, Dextran-spermine-based polyplexes--evaluation of transgene expression and of local and systemic toxicity in mice. *Biomaterials*, 27: 1636-1645, 2006.

[10] H. Eliyahu, A. Makovitzki, T. Azzam, A. Zlotkin, A. Joseph, D. Gazit, Y. Barenholz. A. Domb, Novel dextran–spermine conjugates as transfecting agents: comparing water-soluble and micellar polymers. *Gene therapy*, 12: 494-503, 2005.

[11] H. Farhood, R. Bottega, R.M. Epand. L. Huang, Effect of cationic cholesterol derivatives on gene transfer and protein kinase C activity. *Biochimica et Biophysica Acta (BBA)-Biomembranes*, 1111: 239-246, 1992.

[12] E. Fennema, N. Rivron, J. Rouwkema, C. van Blitterswijk. J. de Boer, Spheroid culture as a tool for creating 3D complex tissues. *Trends in biotechnology*, 31: 108-115, 2013.

[13] J. Friedrich, C. Seidel, R. Ebner. L.A. Kunz-Schughart, Spheroid-based drug screen: considerations and practical approach. *Nature protocols*, 4: 309-324, 2009.

[14] J. Gerdes, H. Lemke, H. Baisch, H.H. Wacker, U. Schwab. H. Stein, Cell cycle analysis of a cell proliferation-associated human nuclear antigen defined by the monoclonal antibody Ki-67. *Journal of immunology*, 133: 1710-1715, 1984.
[15] J.W. Haycock, 3D cell culture: a review of current approaches and techniques. *Methods in molecular biology*, 695: 1-15, 2011.
[16] C.X. He, N. Li, Y.L. Hu, X.M. Zhu, H.J. Li, M. Han, P.H. Miao, Z.J. Hu, G. Wang, W.Q. Liang, Y. Tabata. J.Q. Gao, Effective gene delivery to mesenchymal stem cells based on the reverse transfection and three-dimensional cell culture system. *Pharmaceutical research*, 28: 1577-1590, 2011.
[17] F. Hirschhaeuser, H. Menne, C. Dittfeld, J. West, W. Mueller-Klieser. L.A. Kunz-Schughart, Multicellular tumor spheroids: an underestimated tool is catching up again. *Journal of biotechnology*, 148: 3-15, 2010.
[18] S. Hobel. A. Aigner, Polyethylenimine (PEI)/siRNA-mediated gene knockdown in vitro and in vivo. *Methods in molecular biology*, 623: 283-297, 2010.
[19] H. Hosseinkhani, T. Azzam, H. Kobayashi, Y. Hiraoka, H. Shimokawa, A.J. Domb. Y. Tabata, Combination of 3D tissue engineered scaffold and non-viral gene carrier enhance in vitro DNA expression of mesenchymal stem cells. *Biomaterials*, 27: 4269-4278, 2006.
[20] H. Hosseinkhani, T. Azzam, Y. Tabata. A.J. Domb, Dextran-spermine polycation: an efficient nonviral vector for in vitro and in vivo gene transfection. *Gene therapy*, 11: 194-203, 2004.
[21] M. Ingram, G. Techy, R. Saroufeem, O. Yazan, K. Narayan, T. Goodwin. G. Spaulding, Three-dimensional growth patterns of various human tumor cell lines in simulated microgravity of a NASA bioreactor. *In Vitro Cellular & Developmental Biology-Animal*, 33: 459-466, 1997.
[22] J.M. Kelm. M. Fussenegger, Microscale tissue engineering using gravity-enforced cell assembly. *Trends in biotechnology*, 22: 195-202, 2004.
[23] A. Khademhosseini, J. Yeh, S. Jon, G. Eng, K.Y. Suh, J.A. Burdick. R. Langer, Molded polyethylene glycol microstructures for capturing cells within microfluidic channels. *Lab on a Chip*, 4: 425-430, 2004.
[24] I.A. Khalil, K. Kogure, H. Akita. H. Harashima, Uptake pathways and subsequent intracellular trafficking in nonviral gene delivery. *Pharmacological reviews*, 58: 32-45, 2006.
[25] Q. Kong, G. Wu, L. Han, Z. Zhang, J. Du, W. Sun. L. Cao, A transfection method of PS-asODNs targeting ANGPTL4 in multicellular structures of hepatocarcinoma cell line. *Cancer gene therapy*, 2015.
[26] C.H. Kwon, I. Wheeldon, N.N. Kachouie, S.H. Lee, H. Bae, S. Sant, J. Fukuda, J.W. Kang. A. Khademhosseini, Drug-Eluting Microarrays for Cell-Based Screening of Chemical-Induced Apoptosis. *Analytical Chemistry*, 83: 4118-4125, 2011.
[27] L. Li, J. Sun. Z. He, Deep penetration of nanoparticulate drug delivery systems into tumors: challenges and solutions. *Current medicinal chemistry*, 20: 2881-2891, 2013.
[28] Z. Ma, J. Wang, P. Loskill, N. Huebsch, S. Koo, F.L. Svedlund, N.C. Marks, E.W. Hua, C.P. Grigoropoulos, B.R. Conklin. K.E. Healy, Self-organizing human cardiac microchambers mediated by geometric confinement. *Nature communications*, 6: 7413, 2015.
[29] B. Marrero. R. Heller, The use of an in vitro 3D melanoma model to predict in vivo plasmid transfection using electroporation. *Biomaterials*, 33: 3036-3046, 2012.
[30] B. Marrero. R. Heller, The use of an in vitro 3D melanoma model to predict in vivo plasmid transfection using electroporation. *Biomaterials*, 33: 3036-3046, 2012.

[31] H.R. Mellor, L.A. Davies, H. Caspar, C.R. Pringle, S.C. Hyde, D.R. Gill. R. Callaghan, Optimising non-viral gene delivery in a tumour spheroid model. *The journal of gene medicine*, 8: 1160-1170, 2006.
[32] Y.K. Oh, D. Suh, J.M. Kim, H.G. Choi, K. Shin. J.J. Ko, Polyethylenimine-mediated cellular uptake, nucleus trafficking and expression of cytokine plasmid DNA. *Gene therapy*, 9: 1627-1632, 2002.
[33] M. PV Shekhar, Drug resistance: challenges to effective therapy. *Current cancer drug targets*, 11: 613-623, 2011.
[34] M.T. Santini. G. Rainaldi, Three-dimensional spheroid model in tumor biology. *Pathobiology : journal of immunopathology, molecular and cellular biology*, 67: 148-157, 1999.
[35] T. Scholzen. J. Gerdes, The Ki-67 protein: from the known and the unknown. *Journal of cellular physiology*, 182: 311-322, 2000.
[36] R. Shukla, S. Shukla, V. Bivolarski, I. Iliev, I. Ivanova. A. Goyal, Structural characterization of insoluble dextran produced by Leuconostoc mesenteroides NRRL B-1149 in the presence of maltose. *Food Technology and Biotechnology*, 49: 291-296, 2011.
[37] S. Son. W.J. Kim, Biodegradable nanoparticles modified by branched polyethylenimine for plasmid DNA delivery. *Biomaterials*, 31: 133-143, 2010.
[38] L. Tang, N.P. Gabrielson, F.M. Uckun, T.M. Fan. J. Cheng, Size-dependent tumor penetration and in vivo efficacy of monodisperse drug-silica nanoconjugates. *Molecular pharmaceutics*, 10: 883-892, 2013.
[39] Y.-s. Torisawa, A. Takagi, Y. Nashimoto, T. Yasukawa, H. Shiku. T. Matsue, A multicellular spheroid array to realize spheroid formation, culture, and viability assay on a chip. *Biomaterials*, 28: 559-566, 2007.
[40] Y.-s. Torisawa, A. Takagi, H. Shiku, T. Yasukawa. T. Matsue, A multicellular spheroid-based drug sensitivity test by scanning electrochemical microscopy. *Oncology reports*, 13: 1107-1112, 2005.
[41] M. van der Graaf, R.G. Schipper, G.O. Oosterhof, J.A. Schalken, A.A. Verhofstad. A. Heerschap, Proton MR spectroscopy of prostatic tissue focused on the etection of spermine, a possible biomarker of malignant behavior in prostate cancer. *Magnetic Resonance Materials in Physics, Biology and Medicine*, 10: 153-159, 2000.
[42] W. Wang, K. Itaka, S. Ohba, N. Nishiyama, U.I. Chung, Y. Yamasaki. K. Kataoka, 3D spheroid culture system on micropatterned substrates for improved differentiation efficiency of multipotent mesenchymal stem cells. *Biomaterials*, 30: 2705-2715, 2009.
[43] L. Wasungu, J.-M. Escoffre, A. Valette, J. Teissie. M.-P. Rols, A 3D in vitro spheroid model as a way to study the mechanisms of electroporation. *International journal of pharmaceutics*, 379: 278-284, 2009.
[44] Q.-Q. Zhao, J.-L. Chen, T.-F. Lv, C.-X. He, G.-P. Tang, W.-Q. Liang, Y. Tabata. J.-Q. Gao, N/P ratio significantly influences the transfection efficiency and cytotoxicity of a polyethylenimine/chitosan/DNA complex. *Biol Pharm Bull*, 32: 706-710, 2009.